Stochastic density functional theory at finite temperatures

Yael Cytter
Fritz Haber Center for Molecular Dynamics and Institute of Chemistry, The Hebrew University of Jerusalem, Jerusalem 9190401, Israel

Eran Rabani*
Department of Chemistry, University of California and Lawrence Berkeley National Laboratory, Berkeley, California 94720, USA and The Raymond and Beverly Sackler Center for Computational Molecular and Materials Science, Tel Aviv University, Tel Aviv, Israel 69978

Daniel Neuhauser†
Department of Chemistry, University of California at Los Angeles, California 90095, USA

Roi Baer‡
Fritz Haber Center for Molecular Dynamics and Institute of Chemistry, The Hebrew University of Jerusalem, Jerusalem 9190401, Israel

(Received 7 January 2018; revised manuscript received 14 February 2018; published 27 March 2018)

Simulations in the warm dense matter regime using finite temperature Kohn-Sham density functional theory (FT-KS-DFT), while frequently used, are computationally expensive due to the partial occupation of a very large number of high-energy KS eigenstates which are obtained from subspace diagonalization. We have developed a stochastic method for applying FT-KS-DFT, that overcomes the bottleneck of calculating the occupied KS orbitals by directly obtaining the density from the KS Hamiltonian. The proposed algorithm scales as $O(NT^{-1})$ and is compared with the high-temperature limit scaling $O(N^3T^3)$ of the deterministic approach, where N is the system size (number of electrons, volume, etc.) and T is the temperature. The method has been implemented in a plane-waves code within the local density approximation (LDA); we demonstrate its efficiency, statistical errors, and bias in the estimation of the free energy per electron for a diamond structure silicon. The bias is small compared to the fluctuations and is independent of system size. In addition to calculating the free energy itself, one can also use the method to calculate its derivatives and obtain the equations of state.

DOI: 10.1103/PhysRevB.97.115207

I. INTRODUCTION

Electronic structure calculations coupled with molecular dynamics trajectory sampling form a reliable and important source of information concerning the properties of materials at the warm dense matter (WDM) regime. The main challenges lie in the determination of the equation of state (EOS) of such systems [1–6], addressing their various phase transition boundaries [7,8], and predicting shock-wave propagation characteristics [9–11], as well as their transport and optical properties [12–17].

Reliable and predictive computational approaches should be based on *ab initio* calculations, and these usually fall within the Green's function methods (GF) [18–21], Monte-Carlo (MC) techniques [9,22,23], and density functional theory (DFT) [24–26]. The fact that GF and MC methods are expensive is exacerbated by the need to repeat the electronic calculation for the many nuclear configurations along a molecular dynamics trajectory.

Among the *ab initio* approaches, DFT methods emerge as an ideal framework, combining useful accuracy and applicability. We differentiate between orbital-free DFT [27–32] and finite-temperature Kohn-Sham (FT-KS) approaches [33,34]. The former involves very moderate computational effort but is of limited accuracy due to the use of approximate kinetic energy and entropy functionals. The latter class of DFT approaches on the other hand yields reliable and accurate results and is emerging as the method of choice in the field, with applications ranging from short pulse laser simulations [35,36] and x-ray scattering [37,38] to properties of astrophysical bodies [8,39–41].

The benefits of using the FT-KS method stems from the mapping of the interacting system onto the noninteracting one governed by the single-particle KS Hamiltonian. This, however, comes with a price, since in finite temperature the eigenstates of the KS Hamiltonian are all formally occupied according to the Fermi-Dirac distribution, thus requiring the calculation of all the non-negligibly occupied eigenstates ($N_{\rm occ}$). This numerical task scales typically as $O(N_{\rm occ}^2 N)$, where N indicates the system size (volume, number of electrons, etc.). From the entropy of the noninteracting homogeneous electron gas we find that the proportionality of the number of occupied states with temperature is $N_{\rm occ} \propto NT^{3/2}$, where T is the temperature (in this model the entropy is also proportional to a term that is independent of T, so that in $T = 0$ the number of occupied states goes to a constant. However, one should note that the model only holds in the limit of high temperatures).

*eran.rabani@berkeley.edu
†dxn@chem.ucla.edu
‡roi.baer@huji.ac.il

Consequently, the CPU time of a FT-KS-DFT calculation is expected to scale as $O(T^3N^3)$, which rises rapidly with temperatures and densities of the system. Moreover, it grows significantly when the system is near a phase transition, where physical length scales are large. The purpose of this paper is to propose an alternative implementation of the FT-KS-DFT, based on a stochastic approach [42], in which the CPU time increases linearly with system size and inverse temperature. The scaling of the proposed method is therefore $O(NT^{-1})$ to be compared with the $O(T^3N^3)$ scaling of conventional FT-KS-DFT. Stochastic methods for electronic structure have been developed recently and have shown to be highly efficacious in lowering the algorithmic complexity of a variety of electronic structure calculations [20,43–50]. This paper shows that such an approach can also be useful for research done in WDM and related fields. We focus on the electronic structure aspect of the free energy, neglecting the contribution of the nuclear kinetic energy and entropy, both of which requires an additional effort (such as a molecular dynamics sampling technique). In anticipation of the disorder created by the molecular dynamics sampling, we do not exploit the symmetry of the ordered lattice (as often done by k-point sampling techniques) which we use to demonstrate the method.

We present the method in Sec. II and study its validity by examining the convergence to the known (deterministic) free energy and the stochastic noise accompanying the calculations in Sec. III. In Sec. IV we show how equations of state can be computed in the presence of stochastic noise.

II. METHOD

A. FT-KS-DFT formalism

Consider an ensemble of interacting electrons in inverse temperature $\beta = \frac{1}{k_B T}$ and chemical potential μ. The grand canonical potential operator describing the system would then be

$$\hat{\Omega} = \hat{H} - T\hat{S} - \mu\hat{N}, \tag{1}$$

where $\hat{N}$ is the number of electrons, $\hat{S}$ is the entropy, and $\hat{H}$ is the interacting Hamiltonian, defined as

$$\hat{H} = \hat{T}_{\rm kin} + \hat{v}_{ee} + \hat{v}_{ext};$$

here $\hat{T}_{\rm kin}$ is the total kinetic energy operator, $\hat{v}_{ee}$ represents the interaction between the electrons, and $\hat{v}_{ext}$ is the potential of interaction between the electrons and the nuclei as well as other external fields.

The FT-KS-DFT method maps the interacting system onto an ensemble of noninteracting electrons, the KS system, with the same one-electron density $n(\boldsymbol{r})$ and, commonly though not compulsory, the same inverse temperature β and chemical potential μ [51]. These noninteracting electrons are described by the KS Hamiltonian

$$\hat{h} = -\frac{\hbar^2}{2m_e}\nabla^2 + v_{KS}(\boldsymbol{r}) \tag{2}$$

where m_e is the electron's mass and $\hbar$ is Planck's constant. The potential $v_{KS}(\boldsymbol{r})$ is given by

$$v_{KS}[n](\boldsymbol{r}) = v_{ext}(\boldsymbol{r}) + v_H[n](\boldsymbol{r}) + v_{xc}[n](\boldsymbol{r}), \tag{3}$$

where

$$v_H[n](\boldsymbol{r}) = \int n(\boldsymbol{r}')|\boldsymbol{r} - \boldsymbol{r}'|^{-1}d^3r' \tag{4}$$

is the Hartree potential and $v_{xc}[n](\boldsymbol{r}) = \frac{\delta\Omega_{xc}[n]}{\delta n(\boldsymbol{r})}$ is the exchange-correlation potential, which is a functional derivative of the exchange-correlation grand canonical potential Ω_{xc}. This exchange correlation functional includes the differences between the interacting and noninteracting system's kinetic energy and entropy, as well as the difference between the full Coulomb repulsion energy and the Hartree energy, defined as

$$E_H = \frac{1}{2}\iint \frac{n(\boldsymbol{r})n(\boldsymbol{r}')}{|\boldsymbol{r} - \boldsymbol{r}'|}d^3r'd^3r. \tag{5}$$

The method can be useful if an efficacious approximation to $\Omega_{xc}[n]$ is available. The local density approximation provides such an approximate functional [33]:

$$\Omega_{xc}^{\rm LDA}[n;\beta] = \int \omega_{xc}(n(\boldsymbol{r}),\beta)n(\boldsymbol{r})d^3r \tag{6}$$

$$v_{xc}^{\rm LDA}[n;\beta](\boldsymbol{r}) = \omega_{xc}(n(\boldsymbol{r});\beta) + \omega'_{xc}(n(\boldsymbol{r});\beta)n(\boldsymbol{r}), \tag{7}$$

where $\omega_{xc}(n;\beta)$ is the exchange-correlation free energy per electron for a homogeneous electron gas at density n and inverse temperature β, parameterized based on Monte Carlo free energy calculations [30].

The system's electronic density is given as

$$n(\boldsymbol{r}) = \sum_i f_{\beta,\mu}(\varepsilon_i)|\phi_i(\boldsymbol{r})|^2 \tag{8}$$

$$= {\rm tr}[f_{\beta,\mu}(\hat{h})\hat{n}(\boldsymbol{r})], \tag{9}$$

where $\hat{n}(\boldsymbol{r}) = \delta(\hat{\boldsymbol{r}} - \boldsymbol{r})$ is the electron density operator ($\hat{\boldsymbol{r}}$ is the position of the electron),

$$f_{\beta,\mu}(\varepsilon) = \frac{1}{1 + e^{\beta(\varepsilon-\mu)}} \tag{10}$$

is the Fermi-Dirac distribution, and $\phi_i(\boldsymbol{r})$ (ε_i) is the eigenfunction (eigenvalue) of the self-consistent KS Hamiltonian:

$$\hat{h}\phi_i(\boldsymbol{r}) = \varepsilon_i\phi_i(\boldsymbol{r}). \tag{11}$$

We then construct v_{KS} according to Eq. (3) in order to solve Eq. (11) again. The procedure is repeated until convergence is achieved.

Once the density is obtained, the grand canonical free energy of the interacting system, when the nuclear kinetic energy is neglected [52], is given as:

$$\Omega = \Omega_{KS} - E_H[n] - \int n(\boldsymbol{r})v_{xc}(\boldsymbol{r})d^3r + \Omega_{xc}[n] + E_N, \tag{12}$$

where E_N is the (classical) nuclear-nuclear repulsion energy and

$$\Omega_{KS} = E_{KS} - \mu N - TS_{KS} \tag{13}$$

is the grand canonical potential of the noninteracting system. Here,

$$E_{KS} = {\rm tr}[f_{\beta,\mu}(\hat{h})\hat{h}]. \tag{14}$$

Furthermore,

$$S_{KS} = k_B \mathrm{tr}[f_{\beta,\mu}(\hat{h}) \ln f_{\beta,\mu}(\hat{h}) + \bar{f}_{\beta,\mu}(\hat{h}) \ln \bar{f}_{\beta,\mu}(\hat{h})] \quad (15)$$

is the entropy of the noninteracting electrons where we use the notation $\bar{f} \equiv 1 - f$, and

$$N_e = \int n(\boldsymbol{r}) d^3 r = \mathrm{tr}[f_{\beta,\mu}(\hat{h})]. \quad (16)$$

As can be seen in Eqs. (9) and (14)–(16) all the quantities above can be expressed as traces. The series of iterations involved in the FT-KS-DFT method can then be described in the following manner: A previous guess density $n^{\mathrm{prev}}(\boldsymbol{r})$ is used to construct a KS potential $v_{KS}[n^{\mathrm{prev}}](\boldsymbol{r})$, from which a new guess density $n^{\mathrm{new}}(\boldsymbol{r})$ is obtained:

$$n^{\mathrm{prev}} \underset{\text{Eq. (3)}}{\longrightarrow} v_{KS}[n^{\mathrm{prev}}] \to \hat{h} \underset{\text{Eq. (9)}}{\longrightarrow} n^{\mathrm{new}}(\boldsymbol{r}). \quad (17)$$

These iterations are repeated until the previous and new densities are equal to one another, in which case a self-consistent-field (SCF) density $n(\boldsymbol{r})$ is obtained, so that:

$$n^{\mathrm{prev}} = n^{\mathrm{new}} \equiv n. \quad (18)$$

B. Stochastic approach to FT-KS-DFT

The stochastic approach to FT-KS-DFT (sFT-KS-DFT) exploits the fact that all terms in the free energy of Eq. (13) are expressed using traces over appropriate operators. These traces are then estimated by the stochastic trace formula [53]:

$$\mathrm{tr}[\hat{A}] = \mathrm{E}\{\langle\chi|\hat{A}|\chi\rangle\}, \quad (19)$$

where $\hat{A}$ is an arbitrary operator, χ is a random ket, and $\mathrm{E}\{\cdots\}$ is the statistical average value of the random variable appearing inside the curly brackets. If we use a Cartesian grid of N_g grid points $\boldsymbol{r}$ to represent wave functions and operators in real space then the ket χ is a random orbital and at each grid point $\chi(\boldsymbol{r})$ is a random variable with zero mean, $\mathrm{E}[\{\chi(\boldsymbol{r})\}] = 0$, and a covariance given by

$$\mathrm{E}\{\chi(\boldsymbol{r})\chi(\boldsymbol{r}')^*\} = \Delta^{-3}\delta_{\boldsymbol{r}\boldsymbol{r}'}, \quad (20)$$

where Δ is the grid spacing. This requirement on the random orbital can be achieved by choosing $\chi(\boldsymbol{r}) = \Delta^{-3/2} e^{i\theta(\boldsymbol{r})}$ for each grid point $\boldsymbol{r}$, where $\theta(\boldsymbol{r})$ is an independent random number in the $[0, 2\pi]$ interval.

Assuming the Hamiltonian $\hat{h}$ is known, the FT density can be computed from the trace formula, using I stochastic orbitals χ_i, $i = 1, \ldots, I$ as follows

$$n_I(\boldsymbol{r}) = \frac{1}{I} \sum_{i=1}^{I} |\xi_i(\boldsymbol{r})|^2, \quad (21)$$

where $\xi_i(\boldsymbol{r})$ is a thermally filtered random orbital, given by:

$$\xi_i(\boldsymbol{r}) = \langle \boldsymbol{r}|\Theta_{\beta,\mu}(\hat{h})|\chi_i\rangle, \quad (22)$$

where $\Theta_{\beta,\mu}(\varepsilon) = \sqrt{f_{\beta,\mu}(\varepsilon)}$.

The SCF procedure in the stochastic approach involves a previous stochastic guess density $n_I^{\mathrm{prev}}(\boldsymbol{r})$ and the following process to update it, analogous to Eq. (17):

$$n_I^{\mathrm{prev}} \underset{\text{Eq. (3)}}{\longrightarrow} v_{KS}[n_I^{\mathrm{prev}}] \to \hat{h} \underset{\text{Eq. (21)}}{\longrightarrow} n_I^{\mathrm{new}}(\boldsymbol{r}). \quad (23)$$

These iterations are repeated until the previous and new densities are equal, in which case a self-consistent-field (SCF) density $n_I(\boldsymbol{r})$ is obtained:

$$n_I^{\mathrm{prev}} = n_I^{\mathrm{new}} \equiv n_I. \quad (24)$$

The random density n_I is distributed with a mean $\mathrm{E}\{n_I\}$ and a certain *standard deviation* proportional to $I^{-1/2}$ representing the statistical error. A second part of the statistical error is the *bias*, defined as

$$bias = \mathrm{E}\{n_I\} - n. \quad (25)$$

The origin of the bias is the nonlinear nature of the SCF cycle in Eq. (17) and this error can be shown to diminish asymptotically linearly with I^{-1} (for further reading see Ref. [54]); we will see that is indeed the case in actual calculations presented below. The general conclusion is that as I increases the bias diminishes *faster* than the standard deviation.

C. The Chebyshev expansion

For each $\chi(\boldsymbol{r})$, the calculation of $\xi(\boldsymbol{r})$ employs a Chebyshev polynomial expansion, i.e.,

$$\xi(\boldsymbol{r}) = \sum_{n=0}^{N_C-1} C_n[\Theta_{\beta,\mu}]\phi_n(\boldsymbol{r}), \quad (26)$$

where $\phi_0(\boldsymbol{r}) = \chi(\boldsymbol{r})$, $\phi_1(\boldsymbol{r}) = \hat{h}_N\chi(\boldsymbol{r})$, and for $n > 1$, $\phi_n(\boldsymbol{r}) = 2\hat{h}_N\phi_{n-1}(\boldsymbol{r}) - \phi_{n-2}(\boldsymbol{r})$, with the normalized Hamiltonian

$$\hat{h}_N = \frac{\hat{h} - \frac{1}{2}(E_{\max} + E_{\min})}{\frac{1}{2}(E_{\max} - E_{\min})} = \frac{\hat{h} - \bar{E}}{\Delta E}, \quad (27)$$

where $E_{\max}$ ($E_{\min}$) is an upper bound on the maximal (lower bound on the minimal) eigenvalue of $\hat{h}$. The coefficients $C_n[F]$ are the Chebyshev coefficients corresponding to a function $F(\varepsilon)$ (which is equal to $\Theta_{\beta,\mu}$ in this case). They are given by [55]:

$$C_n = \frac{2 - \delta_{n0}}{2N_C} e^{i\frac{n\pi}{2N_C}} \tilde{F}_n, \quad n = 0, 1, \ldots, N_C - 1, \quad (28)$$

where $\tilde{F}_n$ are the first N_C terms of the fast Fourier transform of the series

$$F_k = F(x_k \Delta E + \bar{E}), \quad k = 0, 1, \ldots, 2N_C - 1, \quad (29)$$

where $x_k = \cos\frac{\pi(k+\frac{1}{2})}{N_C}$. In the case of Eq. (26) we take this function as $F(\varepsilon) = \Theta_{\beta\mu}(\varepsilon)$. The expansion length N_C is selected such that $|C_n| < 10^{-9}$ for $n > N_C$. It can typically be shown that [56]:

$$N_C \propto \beta \Delta E. \quad (30)$$

Since ΔE is half the difference between $E_{\max}$ and $E_{\min}$, where $E_{\max}$ is usually determined by the kinetic energy cutoff and $E_{\min}$ is determined by the ground state screened potential (including the nonlocal part of the pseudopotential), the number of terms in Chebyshev expansion is largely independent of system size.

D. Chebyshev moments

Besides the density, other quantities of interest [see Eqs. (14), (15), and (16)] are all traces of certain functions $F(\hat{h})$

of the KS Hamiltonian $\hat{h}$. The calculation of these quantities can all be expressed as sums of the form:

$$\mathrm{tr}[F(\hat{h})] = \sum_{n=0}^{N_C} C_n[F] M_n, \tag{31}$$

where $C_n[F]$ are the Chebyshev expansion coefficients defined in Eq. (28) and

$$M_n = \mathrm{E}\{\langle\chi|\phi_n\rangle\} \tag{32}$$

are the Chebyshev *moments* [57].

All the results shown in this paper are within the canonical ensemble, having the Helmholtz free energy

$$A(\beta, V, N_e) = \Omega(\beta, \mu, V) + N_e\mu. \tag{33}$$

To obtain a constant number of electrons N_e at each iteration, we include a step of search for the value of μ for which the number of electrons, defined in Eq. (16) and calculated using the moments, is equal to the desired number of electrons. The free energy is then

$$A(\beta, V, N_e) = E_{KS}(\beta, V, \mu(N_e)) - TS_{KS}(\beta, \mu(N_e)) + E_N. \tag{34}$$

The main advantage of the sFT-KS-DFT method is its lower scaling. In the FT-KS-DFT calculation the density is represented as a sum of the square absolute value Kohn-Sham eigenfunctions (each multiplied by its electronic occupation). To calculate these on a grid, one needs to invest $O(N_{\mathrm{occ}}^2 N_g)$ operations and $O(N_{\mathrm{occ}} N_g)$ memory capacity for storage. Since N_{occ} increases quickly with β^{-1} (see discussion in the introduction), the FT-KS-DFT method is a very expensive way to study warm dense matter. In contrast, sFT-KS-DFT requires N_C applications of the KS Hamiltonian $\hat{h}$, to a set of I χ's, a step of order $N_C \times I \times N_g \ln N_g$ floating-point operations (the $\ln N_g$ is due to the fast Fourier transform required for the kinetic energy operation).

In Sec. III we demonstrate how the error per electron, determined by I, does not increase with system size. This is compatible with findings shown in previous work for finite systems described in Ref. [42]. In addition, the prior work demonstrates that as explained in Sec. II C, N_C at a given β is independent of system size as well. Therefore, since I and N_C do not increase with system size the computational effort scales linearly. In addition, since the Chebyshev expansion length N_C is proportional to β [see Eq. (30)], the CPU time actually drops as β decreases (temperature rises) as can be seen in Fig. 1. Moreover, since the procedure is based on averaging over random values of the density, the process of attaining the different values of $n_i(\boldsymbol{r})$ can be done most naturally in parallel.

III. RESULTS: CONVERGENCE AND STATISTICAL ERRORS

The stochastic method described in the previous subsection has been implemented within our *Inbar* [59] plane-waves DFT code and the resulting implementation is dubbed *sInbar*. For demonstrating the code, we use silicon in a FCC diamond structure with periodic boundary conditions described by the ground state local density approximation (LDA). We consider

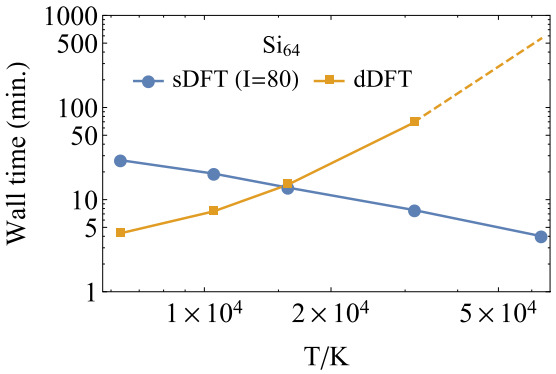

FIG. 1. CPU wall time for self-consistent KS-DFT calculations using the stochastic (sDFT, $I = 80$ stochastic orbitals) and deterministic (single thread dDFT, Quantum Espresso [58]) calculations on Si_{64} having a lattice constant of $21a_0$. The dashed line is the expected $O(T^3)$ extrapolation for the dDFT timings.

Si_8, Si_{64}, Si_{216}, and Si_{512} having respectively 32, 256, 864, and 2048 valence electrons, each using a cubic supercell size of length a, $2a$, $3a$, and $4a$, and the Fourier grid includes N_g, $2^3 N_g$, $3^3 N_g$, and $4^3 N_g$ grid points, respectively, where $N_g = 30^3$. The kinetic energy cutoff is 20 Ry and Troullier-Martins norm-conserving pseudopotentials [60] within the Kleinman-Bylander representation [61] are deployed for describing the electron-nucleus interactions. In the temperature regime used here, based on the results of Ref. [30], it is justified to use ground-state LDA, for which we adopt here the parameterization of Ref. [62].

We now study the nature of the statistical errors in the Helmholtz free energy estimation and their behavior as a function of sampling and system size. In the left panel of Fig. 2 we show the statistics of the Helmholtz free energy per electron $\langle A\rangle/N_e$ estimates as a function of the number of electrons N_e in the unit cell using the four systems presented above at $\beta = 20E_h^{-1}$, keeping the number of stochastic orbitals fixed $I = 80$ (we chose this value for I because results based on it are a good balance between accuracy and computational effort for this system). For each system we use six calculations to estimate the average and standard deviation σ/N_e presented in the figure. As shown in the bottom left hand panel, as system size grows σ/N_e drops in proportion to $N_e^{-1/2}$ in accordance with the self averaging effect [42].

The effect of sample size is studied in the middle panel of Fig. 2, using the Si_{64} system at $\beta = 20E_h^{-1}$ for demonstration. The standard deviation σ/N_e decreases as the sample size grows, roughly in proportion to $I^{-1/2}$ (as in the left panel, we used six independent runs to estimate the mean and the error bars). In addition to the statistical fluctuations the free energy estimate $\langle A\rangle/N_e$ is seen to be biased towards values larger than the deterministic value (dashed line). For $I > 20$ the bias error is found to be smaller than the size of the fluctuation σ/N_e and as shown in the right panel of Fig. 2 the bias decreases linearly with I^{-1} and thus diminishes faster than the fluctuation as I increases, as was also discussed in Sec. II B. It is seen in the right panel of the figure that the bias error in the free energy estimate $\langle A\rangle/N_e$ is largely independent of system size.

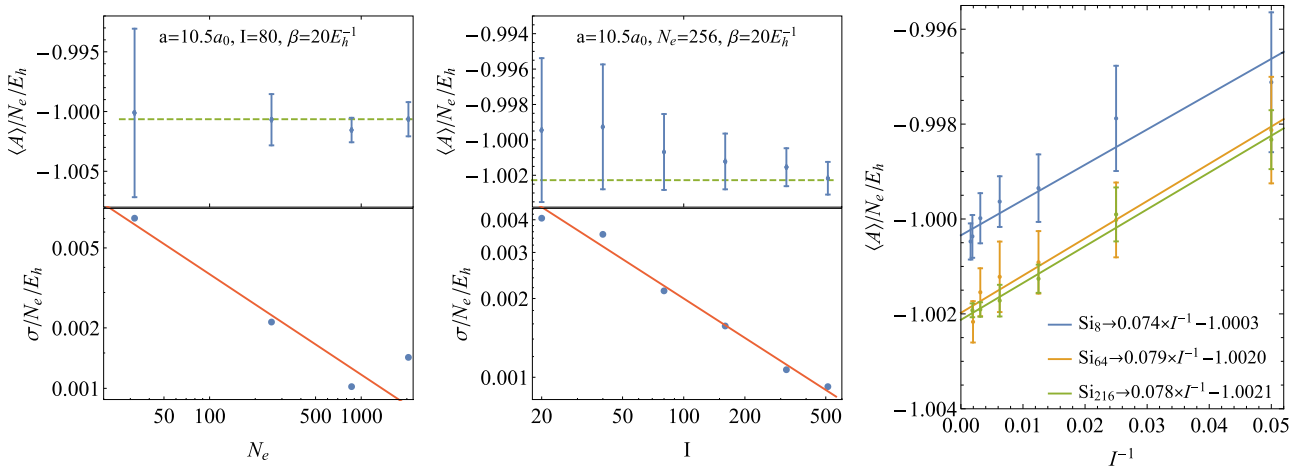

FIG. 2. Left panels: We show in the top left panel the estimated expected value of the Helmholtz free energy per electron (dots) and its square-root-variance σ (half length of error bars $\pm\sigma$ which is also shown in the log plot of the bottom panel) as a function of the number of electrons N_e in four Si supercell sizes (see text) using $I = 80$ stochastic orbitals. The dashed green line is a guide to the eye designating the free energy per electron of the largest system. Middle panels: In the top middle panel we show the estimated expected value of the Helmholtz free energy per electron (dots) and its square-root-variance σ (which is also shown in the log plot of the bottom panel) as a function of the number of stochastic orbitals I for Si_{64}. The dashed green line designates the deterministic value of the free energy per electron for this system. Right panel: The 70% confidence intervals of the estimated Helmholtz free-energy per electron, for several system sizes, as a function of the inverse number of stochastic orbitals I^{-1} the solid lines are best-fit linear curves for the data (their equations are given in the legend).

The free energy as a function of temperature is shown in Fig. 3 where one can see that the statistical fluctuation is not significantly affected by the temperature. Deterministic results are also depicted and once again, the expected values based on statistical estimates are consistently above the deterministic results, showing a temperature-independent statistical bias which is smaller than the fluctuation for $I = 80$.

IV. EQUATION OF STATE CALCULATIONS

In order to calculate thermodynamic properties of the system one needs to take derivatives of the free energy with respect to thermodynamic variables, such as volume and pressure. In the present paper, as was mentioned in Ref. [52],

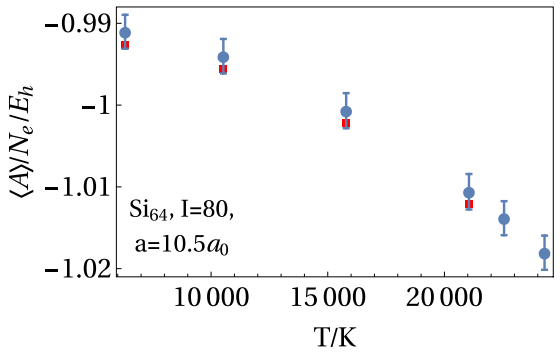

FIG. 3. The estimated expected value of the Helmholtz free energy per electron $\langle A\rangle/N_e$ (dots) and its square-root-variance σ (half length of error bars $\pm\sigma$) for Si_{64} as a function of inverse temperature β, representing a single run of $I = 80$ stochastic orbitals. The expected value and standard deviation were estimated from six independent such runs. The square symbols are the corresponding deterministic values of the free energy.

we do not consider the free energy resulting from the nuclear kinetic energy or entropy. As a result, the equations of state we compute are mostly electronic, and the nuclear position simply comes in as the external potential alongside the nuclear-nuclear repulsion term. Subsequently, we need to define, perhaps arbitrarily, what change needs to be made when we change the system volume. The most natural assumption is to preserve the FCC diamond structure and impose cubic volume changes. The type of free energy obtained from this calculation can be that of a system after exposure to a short and powerful laser pulse, where due to a separation of timescales the nuclei have not yet responded to the external field [7,12].

To address the practical problem of computing derivatives in the presence of stochastic noise we calculate the free energy as a function of a chosen parameter in a *statistically correlated* way. For example, we calculate the free Helmholtz energy $A(\beta, N_e, \rho)$ for a given electron number N_e and inverse temperature β for several discrete values of the density $\rho = N_e/V$, where $V = a^3$ is the cubic simulation cell volume and a is its length. This is done using the same number of Fourier grid points and the same set of random phases for each stochastic orbital on the grid. We demonstrate the results for the Si_{216} system in Fig. 4 corresponding to six independent sets of $I = 80$ stochastic orbitals with which the sFT-KS-DFT calculations were performed. For each set of free energies a third degree polynomial is constructed to best fit the data. It is seen in the top panel of the figure that the free energy data points are well described by the polynomial. A higher order fit does not significantly change the result shown here, indicative of the low level of noise in each separate calculation. The statistical fluctuations are evident in the slightly different shape and shift of the polynomials. The derivatives of each of the free energy polynomials can be used to calculate the corresponding pressure $P = -(\frac{\partial A}{\partial V})_{\beta,N_e}$ and bulk modulus

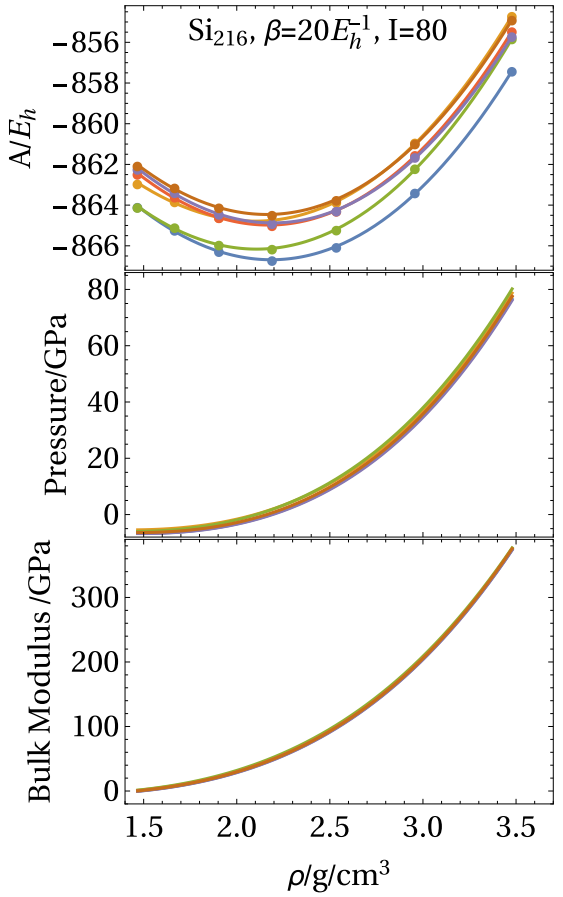

FIG. 4. Top panel: The calculated values of the Helmholtz free energy A for the Si_{216} system (with $N_e = 864$ electrons) at $\beta = 20E_h^{-1}$, at several discrete values of the density $\rho = N_e/V$ (shown as points on plot) calculated for six independent seeds, i.e., each using six sets of $I = 80$ stochastic orbitals. The smooth lines express the free energy $A(\beta, N_e, \rho)$ as a function of ρ using cubic polynomials which best fit the points. Middle and bottom panels: the pressure and bulk modulus isotherms derived from the six free energy curves of the top panel.

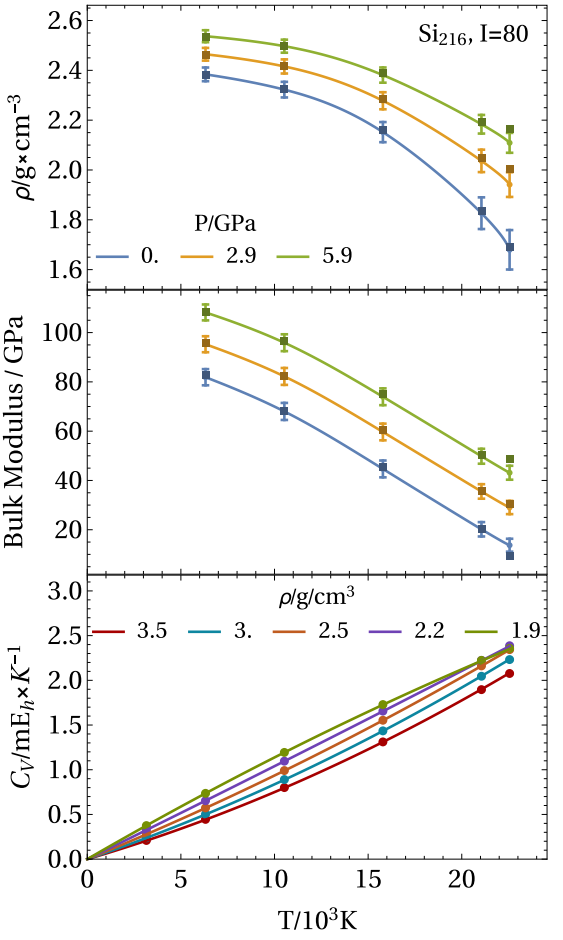

FIG. 5. Top two panels: Isobars of the density (top panel) and bulk modulus (middle panel) in the Si_{216} system, as a function of temperature under different pressures. The stochastic calculations were done using $I = 80$ stochastic orbitals and the data was discerned from the free energy calculations discussed in the text. The darker squares are the results of a stochastic calculation for the Si_{64} system. Bottom panel: The heat capacity for several values of the density as a function of temperature. The error bars are the errors per one seed and are the size of the markers. The lines are the polynomial fits for a specific seed.

$B = -V(\frac{\partial P}{\partial V})_{\beta,N}$, both quantities are plotted, for each set of stochastic calculations, in the middle and lower panels of Fig. 4. The plot gives a sense of the behavior of the statistics of the derivatives which seems well under control, showing that the equations of state of the electrons are accessible using the stochastic approach.

To get a more detailed description of the equation of state and its statistical variance the above procedure is repeated using the same sets of stochastic orbitals, for several values of T. In the top panel of Fig. 5, we show the isobar density ρ as a function of temperature for the Si_{216} system, for several values of the pressure P. The density decreases with increasing temperature and pressure. The results of stochastic calculations for Si_{64} are shown as well (in darker colors) and a size effect, where the density is too high in the small system, is noticeable at high temperatures. We found that this high-temperature-low-density size dependence is due mainly to the entropy term in the free energy.

From the results shown in the figure, it is apparent that the standard deviation in the calculations does not change as a function of temperature, enabling good resolution with a clearly visible trend. We see that regardless of the pressure, the density decreases with temperature, i.e., the system expands.

The bulk modulus shown in the bottom panel of Fig. 5 seems to decrease as we go to higher temperatures, up until the point where it is roughly estimated to vanish at $T \approx 26\,000$ K, at this point the density will be very low. The implication of these results for fast electron heating by powerful lasers is that at short time scales after the pulse, when nuclei are still cold, the material can retain its elasticity even in temperatures of up to 20 000 K. This concept has been investigated both theoretically and experimentally in relation to nonthermal melting [63–65], where the potential energy surface changes as a result of excitation of a large fraction of the valence electrons to the conductance band. Previous work showed that neglecting

electron-phonon interactions leads to overestimation of the phase transition threshold in silicon [64], a matter that could explain our results. In this paper, however, our calculations are restricted to examination of the breathing mode. To further explore the subject, molecular dynamics has to be employed.

The heat capacity $C_V = -T(\frac{d^2A}{dT^2})$ is shown in Fig. 5 exhibiting low statistical noise that is hardly noticeable in the tested scales. We see that the heat capacity grows almost linearly with temperature and goes to zero as $T \to 0$, in accordance with the third law of thermodynamics applying for perfect crystals. To validate the calculation, we changed the polynomial degree of the fit from third to fifth order and saw almost no difference in the heat capacity's behavior as a function of the displayed temperatures. At higher temperatures, however, the fit becomes more sensitive to the polynomial order, an effect amplified when looking at its second derivative. This is a result of the steep decrease of the free energy as temperature increases, as seen in Fig. 3. To avoid the inconsistency, at higher temperature range the free energy has to be sampled more frequently.

V. SUMMARY

In this paper we introduced the stochastic approach for FT-KS-DFT calculations to the warm dense matter regime. We analyzed the statistical errors associated with the stochastic calculations and their dependence on the number of iterations I, the system size and various parameters such as the temperature and the density. We found that the fluctuations in the estimates of the intensive properties decrease as $I^{-1/2}$ and as system size grows. The bias errors, resulting from the nonlinear nature of the self consistent-field procedure, do not grow with system size and decay as I^{-1}. In general, the bias errors turned out to be small for the systems studied here. Furthermore, while both errors do not depend on the temperature, calculation time is inversely proportional to it, making the method highly efficient in the high temperature regime. It has also been shown that the Helmholtz free energy $A(\beta,\rho,N_e)$ can be computed as a smooth and well-behaved function of its variables provided the same set of stochastic orbitals are used. By exploiting this feature, we demonstrated that the equations of state and the associated properties, such as the pressure, heat capacity, and bulk modulus become accessible as derivatives. Our calculations did not use the symmetry properties that allow efficient k-point sampling to be utilized, in anticipation of the realistic cases where high temperature is associated with disorder and nonsymmetry.

Future work in the field will include an implementation to molecular dynamics sampling of the nuclear properties. Such an approach has recently been shown viable at low temperatures using embedded fragments which lower the statistical errors [48]. An additional future direction will examine the use of potential functional theory [28,66] for WDM calculations, where we will study the possibility of lowering the variance by using a coupling constant integration instead of a trace over the kinetic energy operator.

ACKNOWLEDGMENT

We gratefully acknowledge the support of the Israel-USA Binational Science Foundation (US), Grant No. 2015687.

[1] J. Clérouin, P. Renaudin, Y. Laudernet, P. Noiret, and M. P. Desjarlais, Electrical conductivity and equation-of-state study of warm dense copper: Measurements and quantum molecular dynamics calculations, Phys. Rev. B **71**, 064203 (2005).

[2] P. M. Kowalski, S. Mazevet, D. Saumon, and M. Challacombe, Equation of state and optical properties of warm dense helium, Phys. Rev. B **76**, 075112 (2007).

[3] N. Nettelmann, B. Holst, A. Kietzmann, M. French, R. Redmer, and D. Blaschke, Ab initio equation of state data for hydrogen, helium, and water and the internal structure of jupiter, Astrophys. J. **683**, 1217 (2008).

[4] E. G. Saiz, G. Gregori, D. O. Gericke, J. Vorberger, B. Barbrel, R. J. Clarke, R. R. Freeman, S. H. Glenzer, F. Y. Khattak, M. Koenig *et al.*, Probing warm dense lithium by inelastic x-ray scattering, Nat. Phys. **4**, 940 (2008).

[5] G. Faussurier, C. Blancard, P. Cossé, and P. Renaudin, Equation of state, transport coefficients, and stopping power of dense plasmas from the average-atom model self-consistent approach for astrophysical and laboratory plasmas, Phys. Plasmas **17**, 052707 (2010).

[6] M. A Morales, C. Pierleoni, and D. M. Ceperley, Equation of state of metallic hydrogen from coupled electron-ion monte carlo simulations, Phys. Rev. E **81**, 021202 (2010).

[7] R. Ernstorfer, M. Harb, C. T. Hebeisen, G. Sciaini, T. Dartigalongue, and R. J. D. Miller, The formation of warm dense matter: Experimental evidence for electronic bond hardening in gold, Science (Washington, DC, U. S.) **323**, 1033 (2009).

[8] M. D. Knudson, M. P. Desjarlais, A. Becker, R. W. Lemke, K. R. Cochrane, M. E. Savage, D. E. Bliss, T. R. Mattsson, and R. Redmer, Direct observation of an abrupt insulator-to-metal transition in dense liquid deuterium, Science **348**, 1455 (2015).

[9] B. Militzer, D. M. Ceperley, J. D. Kress, J. D. Johnson, L. A. Collins, and S. Mazevet, Calculation of a Deuterium Double Shock Hugoniot from *ab Initio* Simulations, Phys. Rev. Lett. **87**, 275502 (2001).

[10] M. W. C. Dharma-Wardana, Static and dynamic conductivity of warm dense matter within a density-functional approach: Application to aluminum and gold, Phys. Rev. E **73**, 036401 (2006).

[11] V. B. Mintsev and V. E. Fortov, Transport properties of warm dense matter behind intense shock waves, Laser Part. Beams **33**, 41 (2015).

[12] B. Nagler, U. Zastrau, R. R. Fäustlin, S. M. Vinko, T. Whitcher, A. J. Nelson, R. Sobierajski, J. Krzywinski, J. Chalupsky, E. Abreu, S. Bajt, T. Bornath, T. Burian, H. Chapman, J. Cihelka, T. Döppner, S. Düsterer, T. Dzelzainis, M. Fajardo, E. Förster, C. Fortmann, E. Galtier, S. H. Glenzer, S. Göde, G. Gregori, V. Hajkova, P. Heimann, L. Juha, M. Jurek, F. Y. Khattak, A. R. Khorsand, D. Klinger, M. Kozlova, T. Laarmann, H. J. Lee, R. W. Lee, K. H. Meiwes-Broer, P. Mercere, W. J. Murphy, A. Przystawik, R. Redmer, H. Reinholz, D. Riley, G. Röpke, F. Rosmej, K. Saksl, R. Schott, R. Thiele, J. Tiggesbäumker, S. Toleikis, T. Tschentscher, I. Uschmann, H. J. Vollmer, and J. S.

Wark, Turning solid aluminium transparent by intense soft x-ray photoionization, Nat. Phys. **5**, 693 (2009).
[13] V. Vlček, N. de Koker, and G. Steinle-Neumann, Electrical and thermal conductivity of al liquid at high pressures and temperatures from *ab initio* computations, Phys. Rev. B **85**, 184201 (2012).
[14] J. Clérouin, P. Noiret, P. Blottiau, V. Recoules, B. Siberchicot, P. Renaudin, C. Blancard, G. Faussurier, B. Holst, and C. E. Starrett, A database for equations of state and resistivities measurements in the warm dense matter regime, Phys. Plasmas **19**, 082702 (2012).
[15] D. Pan, L. Spanu, B. Harrison, D. A. Sverjensky, and G. Galli, Dielectric properties of water under extreme conditions and transport of carbonates in the deep earth, Proc. Natl. Acad. Sci. U.S.A. **110**, 6646 (2013).
[16] E. M. Apfelbaum, The electron transport coefficients of boron and silicon plasma, Contrib. Plasma Phys. **53**, 317 (2013).
[17] S. A. Sato, Y. Shinohara, T. Otobe, and K. Yabana, Dielectric response of laser-excited silicon at finite electron temperature, Phys. Rev. B **90**, 174303 (2014).
[18] S. V. Faleev, M. van Schilfgaarde, T. Kotani, F. Léonard, and M. P. Desjarlais, Finite-temperature quasiparticle self-consistent *GW* approximation, Phys. Rev. B **74**, 033101 (2006).
[19] A. A. Kananenka, J. J. Phillips, and D. Zgid, Efficient temperature-dependent Green's functions methods for realistic systems: Compact grids for orthogonal polynomial transforms, J. Chem. Theory Comput. **12**, 564 (2016).
[20] D. Neuhauser, R. Baer, and D. Zgid, Stochastic self-consistent second-order Green's function method for correlation energies of large electronic systems, J. Chem. Theory Comput. **13**, 5396 (2017).
[21] J. J. Kas and J. J. Rehr, Finite Temperature Green's Function Approach for Excited State and Thermodynamic Properties of Cool to Warm Dense Matter, Phys. Rev. Lett. **119**, 176403 (2017).
[22] K. P. Driver and B. Militzer, All-Electron Path Integral Monte Carlo Simulations of Warm Dense Matter: Application to Water and Carbon Plasmas, Phys. Rev. Lett. **108**, 115502 (2012).
[23] E. Brown, M. A. Morales, C. Pierleoni, and D. Ceperley, Quantum monte carlo techniques and applications for warm dense matter, in *Frontiers and Challenges in Warm Dense Matter*, edited by Frank Graziani, Michael P. Desjarlais, Ronald Redmer, and Samuel B. Trickey (Springer International Publishing, Cham, 2014), pp. 123–149.
[24] P. Hohenberg and W. Kohn, Inhomogeneous electron gas, Phys. Rev. **136**, B864 (1964).
[25] N. D. Mermin, Thermal properties of the inhomogeneous electron gas, Phys. Rev. **137**, A1441 (1965).
[26] A. Pribram-Jones, S. Pittalis, E. K. U. Gross, and K. Burke, Thermal density functional theory in context, in *Frontiers and Challenges in Warm Dense Matter* (Springer, Cham, 2014), pp. 25–60.
[27] Y. A. Wang, N. Govind, and E. A. Carter, Orbital-free kinetic-energy functionals for the nearly free electron gas, Phys. Rev. B **58**, 13465 (1998).
[28] A. Cangi and A. Pribram-Jones, Efficient formalism for warm dense matter simulations, Phys. Rev. B **92**, 161113 (2015).
[29] V. V. Karasiev, T. Sjostrom, and S. B. Trickey, Generalized-gradient-approximation noninteracting free-energy functionals for orbital-free density functional calculations, Phys. Rev. B **86**, 115101 (2012).
[30] V. V. Karasiev, T. Sjostrom, J. Dufty, and S. B. Trickey, Accurate Homogeneous Electron Gas Exchange-Correlation free Energy for Local Spin-Density Calculations, Phys. Rev. Lett. **112**, 076403 (2014).
[31] V. V. Karasiev and S. B. Trickey, Chapter nine-frank discussion of the status of ground-state orbital-free dft, Adv. Quantum Chem. **71**, 221 (2015).
[32] T. Sjostrom and J. Daligault, Fast and Accurate Quantum Molecular Dynamics of Dense Plasmas Across Temperature Regimes, Phys. Rev. Lett. **113**, 155006 (2014).
[33] W. Kohn and L. J. Sham, Self-consistent equations including exchange and correlation effects, Phys. Rev. **140**, A1133 (1965).
[34] S. Pittalis, C. R. Proetto, A. Floris, A. Sanna, C. Bersier, K. Burke, and E. K. U. Gross, Exact Conditions in Finite-Temperature Density-Functional Theory, Phys. Rev. Lett. **107**, 163001 (2011).
[35] P. L. Silvestrelli, A. Alavi, M. Parrinello, and D. Frenkel, *Ab Initio* Molecular Dynamics Simulation of Laser Melting of Silicon, Phys. Rev. Lett. **77**, 3149 (1996).
[36] A. Kietzmann, R. Redmer, M. P. Desjarlais, and T. R. Mattsson, Complex Behavior of Fluid Lithium Under Extreme Conditions, Phys. Rev. Lett. **101**, 070401 (2008).
[37] K. U. Plagemann, P. Sperling, R. Thiele, M. P. Desjarlais, C. Fortmann, T. Döppner, H. J. Lee, S. H. Glenzer, and R. Redmer, Dynamic structure factor in warm dense beryllium, New J. Phys. **14**, 055020 (2012).
[38] A. D. Baczewski, L. Shulenburger, M. P. Desjarlais, S. B. Hansen, and R. J. Magyar, X-ray Thomson Scattering In Warm Dense Matter without the Chihara Decomposition, Phys. Rev. Lett. **116**, 115004 (2016).
[39] M. Bethkenhagen, E. R. Meyer, S. Hamel, N. Nettelmann, M. French, L. Scheibe, C. Ticknor, L. A. Collins, J. D. Kress, J. J. Fortney *et al.*, Planetary ices and the linear mixing approximation, Astrophys. J. **848**, 67 (2017).
[40] A. Alavi, M. Parrinello, and D. Frenkel, *Ab initio* calculation of the sound velocity of dense hydrogen: Implications for models of Jupiter, Science **269**, 1252 (1995).
[41] M. Schöttler, M. French, D. Cebulla, and R. Redmer, Free energy model for solid high-pressure phases of carbon, J. Phys.: Condens. Matter **28**, 145401 (2016).
[42] R. Baer, D. Neuhauser, and E. Rabani, Self-Averaging Stochastic Kohn-Sham Density-Functional Theory, Phys. Rev. Lett. **111**, 106402 (2013).
[43] D. Neuhauser, Y. Gao, C. Arntsen, C. Karshenas, E. Rabani, and R. Baer, Breaking the Theoretical Scaling Limit for Predicting Quasiparticle Energies: The Stochastic GW Approach, Phys. Rev. Lett. **113**, 076402 (2014).
[44] D. Neuhauser, E. Rabani, and R. Baer, Expeditious stochastic calculation of random-phase approximation energies for thousands of electrons in three dimensions, J. Phys. Chem. Lett. **4**, 1172 (2013).
[45] D. Neuhauser, E. Rabani, and R. Baer, Expeditious stochastic approach for MP2 energies in large electronic systems, J. Chem. Theory Comput. **9**, 24 (2013).
[46] D. Neuhauser, R. Baer, and E. Rabani, Communication: Embedded fragment stochastic density functional theory, J. Chem. Phys. **141**, 041102 (2014).

[47] D. Neuhauser, E. Rabani, Y. Cytter, and R. Baer, Stochastic optimally tuned range-separated hybrid density functional theory, J. Phys. Chem. A **120**, 3071 (2015).

[48] E. Arnon, E. Rabani, D. Neuhauser, and R. Baer, Equilibrium configurations of large nanostructures using the embedded saturated-fragments stochastic density functional theory, J. Chem. Phys. **146**, 224111 (2017).

[49] E. Rabani, R. Baer, and D. Neuhauser, Time-dependent stochastic bethe-salpeter approach, Phys. Rev. B **91**, 235302 (2015).

[50] T. Y. Takeshita, W. A. de Jong, D. Neuhauser, R. Baer, and E. Rabani, Stochastic formulation of the resolution of identity: Application to second order Møller–Plesset perturbation theory, J. Chem. Theory Comput. **13**, 4605 (2017).

[51] R. G. Parr and W. Yang, *Density Functional Theory of Atoms and Molecules* (Oxford University Press, Oxford, 1989).

[52] Throughout the paper, the free energy shown is equal to the electronic free energy plus the nuclear Coulomb interaction energy, with the nuclei positions assuming those of the silicon diamond structure appropriate for each unit cell size. This neglect of the nuclear kinetic energy and entropy allows us to focus on the stochastic approach concerning the contribution of the electrons to the free energy. Furthermore it may be relevant for cases where the electrons are heated very fast (with a strong and short laser pulse) while the nuclei remains cold.

[53] M. F. Hutchinson, A stochastic estimator of the trace of the influence matrix for laplacian smoothing splines, Commun. Stat. Simul. Comput. **19**, 433 (1990).

[54] G. Bohm and G. Zech, *Introduction to Statistics and Data Analysis for Physicists*, Vol. 1 (DESY, Hamburg, 2010).

[55] W. H. Press, W. T. Vetterling, S. A. Teukolsky, and B. P. Flannery, *Numerical Recipes 3rd Edition: The Art of Scientific Computing* (Cambridge University Press, Cambridge, 2007).

[56] R. Baer and M. Head-Gordon, Sparsity of the Density Matrix in Kohn-Sham Density Functional Theory and an Assessment of Linear System-Size Scaling Methods, Phys. Rev. Lett. **79**, 3962 (1997).

[57] L. W. Wang, Calculating the density-of-states and optical-absorption spectra of large quantum-systems by the plane-wave moments method, Phys. Rev. B **49**, 10154 (1994).

[58] P. Giannozzi, S. Baroni, N. Bonini, M. Calandra, R. Car, C. Cavazzoni, D. Ceresoli, G. L. Chiarotti, M. Cococcioni, I. Dabo, A. D. Corso, S. de Gironcoli, S. Fabris, G. Fratesi, R. Gebauer, U. Gerstmann, C. Gougoussis, A. Kokalj, M. Lazzeri, L. Martin-Samos, N. Marzari, F. Mauri, R. Mazzarello, S. Paolini, A. Pasquarello, L. Paulatto, C. Sbraccia, S. Scandolo, G. Sclauzero, A. P. Seitsonen, A. Smogunov, P. Umari, and R. M. Wentzcovitch, Quantum espresso: A modular and open-source software project for quantum simulations of materials, J. Phys.: Condens. Matter **21**, 395502 (2009).

[59] *Inbar* (Hebrew), *anbar* (Arabic), *amber* or *ēlectrum* (Latin) and *electron* in Greek is the yellow-brownish fossil resin of vegetable origin negatively charged by friction.

[60] N. Troullier and J. L. Martins, Efficient pseudopotentials for plane-wave calculations, Phys. Rev. B **43**, 1993 (1991).

[61] L. Kleinman and D. M. Bylander, Efficacious form for Model Pseudopotentials, Phys. Rev. Lett. **48**, 1425 (1982).

[62] J. P. Perdew and Y. Wang, Accurate and simple analytic representation of the electron-gas correlation-energy, Phys. Rev. B **45**, 13244 (1992).

[63] K. Sokolowski-Tinten, C. Blome, J. Blums, A. Cavalleri, C. Dietrich, A. Tarasevitch, I. Uschmann, E. Forster, M. Kammler, M. Horn-von Hoegen, and D. Von der Linde, Femtosecond x-ray measurement of coherent lattice vibrations near the Lindemann stability limit, Nature (London) **422**, 287 (2003).

[64] Z. B. Medvedev N and Li Z, Thermal and nonthermal melting of silicon under femtosecond x-ray irradiation, Phys. Rev. B **91**, 054113 (2015).

[65] A. Rousse, C. Rischel, S. Fourmaux, I. Uschmann, S. Sebban, G. Grillon, P. Balcou, E. Forster, J. Geindre, P. Audebert, J. Gauthier, and D. Hulin, Non-thermal melting in semiconductors measured at femtosecond resolution, Nature **410**, 65 (2001).

[66] A. Cangi, D. Lee, P. Elliott, K. Burke, and E. K. U. Gross, Electronic Structure via Potential Functional Approximations, Phys. Rev. Lett. **106**, 236404 (2011).